(2)

REPORT DOCUMENTATION PAGE

1a. REPORT SECURITY CLASSIFICATION: UNCLASSIFIED	1b. RESTRICTIVE MARKINGS
2a. SECURITY CLASSIFICATION AUTHORITY	3. DISTRIBUTION / AVAILABILITY OF REPORT: This document has been approved for public release and sale; distribution of this document is unlimited.
2b. DECLASSIFICATION / DOWNGRADING SCHEDULE	
4. PERFORMING ORGANIZATION REPORT NUMBER(S): 73	5. MONITORING ORGANIZATION REPORT NUMBER(S)
6a. NAME OF PERFORMING ORGANIZATION: Regents of the U. of California; 6b. OFFICE SYMBOL (If applicable): 4B557	7a. NAME OF MONITORING ORGANIZATION: Office of Naval Research
6c. ADDRESS (City, State, and ZIP Code): University of California, 405 Hilgard Ave., Los Angeles, CA 90024	7b. ADDRESS (City, State, and ZIP Code): Branch Office, 567 South Wilson Street, Pasadena, CA 91106
8a. NAME OF FUNDING / SPONSORING ORGANIZATION: Office of Naval Research; 8b. OFFICE SYMBOL (If applicable): N00014	9. PROCUREMENT INSTRUMENT IDENTIFICATION NUMBER: N00014-89-J-1350
8c. ADDRESS (City, State, and ZIP Code): Chemistry Branch, Arlington, Virginia 22217	10 SOURCE OF FUNDING NUMBERS: PROGRAM ELEMENT NO. / PROJECT NO. / TASK NO. / WORK UNIT ACCESSION NO.

11. TITLE (Include Security Classification) UNCLASSIFIED

Photodissociation of CF_3I at 304 nm: Effects of Photon Energy and Curve Crossing on the Internal Excitation of CF_3

12. PERSONAL AUTHOR(S)

Hyun Jin Hwang and M. A. El-Sayed

13a. TYPE OF REPORT	13b. TIME COVERED FROM ____ TO ____	14. DATE OF REPORT (Year, Month, Day)	15. PAGE COUNT
			38

16. SUPPLEMENTARY NOTATION

Submitted to the Journal of Physical Chemistry

17. COSATI CODES			18. SUBJECT TERMS (Continue on reverse if necessary and identify by block number)
FIELD	GROUP	SUB-GROUP	

19. ABSTRACT (Continue on reverse if necessary and identify by block number)

We present correlated measurements of the CF_3 internal energy, the initial electronic excitation, and the final iodine state in the photodissociation of CF_3I at 304 nm by using state-selective photofragment translational spectroscopy. The simulataneous determination of the three properties is achieved by measuring the translational energy distribution of the state-selected iodine fragment as a function of its recoil angle with respect to the electric vector of the photolysis laser. We found that the excited state I^* ($^2P_{1/2}$)atoms are formed predominantly from the parallel $^3Q_0$–N transition while the I($^2P_{3/2}$)atoms are formed from both the perpendicular $^3Q_1$–N transition (70%) and the parallel $^3Q_0$–N transition (30%) followed by curve crossing to the $^1Q_1$ state. By comparing the average internal energies of CF_3 produced in the two dissociation channels of the $^3Q_0$–N excitation at 304 nm with the recent results of Felder at 248 nm, we examine the effect of the photon energy and that of the curve crossing in the dynamics of the vibrational excitation. For the I^* channel, we observe a strong photon energy dependence of the CF_3 internal excitation, suggesting a strong final state interaction in the dynamics of the $^3Q_0$ potential as suggested by a number of model calculations. The best agreement obtained with the model calculation of van Veen et al. supports the assumption of the dominant involvement of the 1/2 umbrella vibration. For the $^3Q_0$ component of the I channel, we observe a similar strong photon energy dependence in terms of its slope, but with an enhanced CF_3 internal excitation. This suggests the importance of the curve crossing dynamics as well as the dynamics of the $^1Q_1$ potential. The gross disagreement obtained with the one-dimensional model calculation of van Veen et al. is attributed to the multidimensional nature of the curve crossing process.

20. DISTRIBUTION / AVAILABILITY OF ABSTRACT	21. ABSTRACT SECURITY CLASSIFICATION	
☒ UNCLASSIFIED/UNLIMITED ☐ SAME AS RPT. ☐ DTIC USERS	UNCLASSIFIED	
22a NAME OF RESPONSIBLE INDIVIDUAL: M. A. EL-SAYED	22b. TELEPHONE (Include Area Code): (213) 825-1352	22c. OFFICE SYMBOL

DD FORM 1473, 84 MAR — 83 APR edition may be used until exhausted. All other editions are obsolete.

SECURITY CLASSIFICATION OF THIS PAGE: UNCLASSIFIED

OFFICE OF NAVAL RESEARCH

GRANT N00014-89-J-1350

R&T Code 4131015

Technical Report No. 72

Photodissociation of CF_3I at 304 nm: Effects of Photon Energy and Curve Crossing on the Internal Excitation of CF_3

by

Hyun Jin Hwang and M. A. El-Sayed

Submitted to the Journal of Physical Chemistry

University of California
Department of Chemistry and Biochemistry
Los Angeles, California 90024

May 27, 1992

Photodissociation of CF_3I at 304 nm: Effects of Photon Energy and Curve Crossing on the Internal Excitation of CF_3

Hyun Jin Hwang[†] and Mostafa A. El-Sayed*

Department of Chemistry and Biochemistry, University of California, Los Angeles, California 90024

Abstract

We present correlated measurements of the CF_3 internal energy, the initial electronic excitation, and the final iodine state in the photodissociation of CF_3I at 304 nm by using state-selective photofragment translational spectroscopy. The simultaneous determination of the three properties is achieved by measuring the translational energy distribution of the *state-selected* iodine fragment as a function of its recoil angle with respect to the electric vector of the photolysis laser. We found that the excited state $I^*(^2P_{1/2})$ atoms are formed predominantly from the parallel $^3Q_0 \leftarrow N$ transition while the $I(^2P_{3/2})$ atoms are formed from both the perpendicular $^3Q_1 \leftarrow N$ transition (70%) and the parallel $^3Q_0 \leftarrow N$ transition (30%) followed by curve crossing to the $^1Q_1$ state. By comparing the average internal energies of CF_3 produced in the two dissociation channels of the $^3Q_0 \leftarrow N$ excitation at 304 nm with the recent results of Felder at 248 nm, we examine the effect of the photon energy and that of the curve crossing in the dynamics of the vibrational excitation. For the I^* channel, we observe a strong photon energy dependence of the CF_3 internal excitation, suggesting a strong final state interaction in the dynamics of the $^3Q_0$ potential as suggested by a number of model calculations. The best agreement obtained with the model calculation of van Veen *et al.* supports the assumption of the dominant involvement of the

---

[†] Present address: Department of Chemistry, University of California, Berkeley, CA 94720.

ν_2 umbrella vibration. For the $^3Q_0$ component of the I channel, we observe a similar strong photon energy dependence in terms of its slope, but with an enhanced CF_3 internal excitation. This suggests the importance of the curve crossing dynamics as well as the dynamics of the $^1Q_1$ potential. The gross disagreement obtained with the one-dimensional model calculation of van Veen *et al.* is attributed to the multidimensional nature of the curve crossing process.

I. Introduction

Methyl iodide CH_3I and its substituted analogues CD_3I and CF_3I have received a substantial attention as excellent model systems for investigating the photodissociation dynamics of polyatomic molecules.[1-6] The photodissociation of these molecules (CX_3I) in their first absorption band (the so-called *A* band) is particularly interesting since the dynamics of the vibrational excitation during the simple C-I bond rupture is relatively well confined in only one vibrational mode (the ν_2 umbrella bending vibration of CX_3)[1,4,7] due to very fast dissociation[8,9] and the C_{3v} geometry. This has offered a unique opportunity to theoreticians to model detailed photodissociation dynamics under the simplified assumption[10] of "collinear pseudotriatomic dissociation". It is thus not surprising that the vibrational distribution of the CX_3 fragment has been one of the most important subjects in both experiment[3,4,11-15] and theory.[1,3,5,6,10] Another important factor in the photodissociation dynamics of CX_3I is a nonadiabatic curve crossing between two (out of three) radiatively accessible electronic states which correlate to different electronic states of the iodine fragment.[2] Due to the presence of this process and the possibility of exciting multiple electronic states, detailed investigation for the dynamics of the vibrational excitation requires measurements of the vibrational distribution of the CX_3 fragment in correlation with the initial excitation and the final state of the iodine fragment.

In this work, we investigate the photodissociation of CF_3I at ~304 nm with a particular emphasis on the simultaneous determination of the CF_3 internal excitation, the initial electronic excitation, and the final state of the iodine fragment. The experimental basis of this work has been provided by our recent work[16] on the photodissociation of a larger analogous molecule C_2F_5I at ~304 nm. We use a technique of state-selective photofragment translational spectroscopy in combination with a polarized-laser photolysis.[16-18] The simultaneous determination of the three properties is achieved by measuring the translational energy distribution of the state-selected iodine fragment as a function of its recoil angle with respect to the electric vector of the photolysis laser. Combining this type of measurements with the known nature of the electronic transitions in the *A* band, we identify both the initial excitation and the final state of the iodine fragment while determining the internal energy distribution of the CF_3 fragment from the translational energy distribution of the iodine fragment. We will compare the results of this work at ~304 nm with the recent results of Felder[4(b)] at 248 nm to examine the effect of photon energy and that of the curve crossing in the dynamics of the vibrational excitation. Some details of these effects will be deduced by comparing with theoretical predictions from model calculations.[3,5,6]

II. Previous Results

Photoexcitation of CX_3I in the *A* band (350 nm - 200 nm) results in prompt dissociation[8,9] along the C-I bond due to the repulsive nature of the excited states, producing a ground state CX_3 radical and either a spin-orbit excited state I^* ($^2P_{1/2}$) or a ground state I ($^2P_{3/2}$) atom.[19,20] As first discussed by Mulliken,[21] the *A* band of CX_3I arises from the $\sigma^* \leftarrow n$ transition localized in the C-I bond and consists of three overlapping transitions from the ground *N* state to the $^3Q_1$ $^3Q_0$, and $^1Q_1$ states in order of increasing energy. The transition to the $^3Q_0$ state, which is of A_1 symmetry in the C_3 geometry, is

polarized parallel to the C-I bond and correlates to formation of the I^* atom. The transitions to the $^3Q_1$ and $^1Q_1$ states (of *E* symmetry) are polarized perpendicular to the C-I bond and correlate to formation of the I atom. The three components of the *A* band of CH_3I (Ref. 22) and CF_3I (Ref. 23) have been resolved by Gedanken and Rowe using magnetic circular dichroism (MCD). The MCD results revealed that the $^3Q_0$ state carries most of the oscillator strength (78% and 84% for CH_3I and CF_3I, respectively) and has its absorption maximum near 260 nm. Absorption maxima of the $^1Q_1$ and $^3Q_1$ states were found to be located around 240 and 300 nm, respectively. From time-of-flight (TOF) photofragment translational spectroscopy studies[11-13,20] on CH_3I at 266 and 248 nm, it was found that the I atom is produced mainly by a nonadiabatic curve crossing from the $^3Q_0$ to the $^1Q_1$ state and absorption is almost exclusively to the $^3Q_0$ state in gross disagreement with the MCD results. In the case of CF_3I at 248 nm, both the $^3Q_0$ and $^1Q_1$ states were found to contribute to absorption and also formation of both I and I^* atoms due to the curve crossing.[3,4,24]

So far, the internal energy distribution of the CF_3 fragment from the photodissociation of CF_3I has been measured at only one wavelength 248 nm by two groups.[3,4] van Veen *et al.*,[3] using the TOF photofragment translational spectroscopy, first determined the CF_3 vibrational distribution at 248 nm from the measured translational energy distribution under the assumption that the ν_2 umbrella vibration is the only mode excited as observed in the CH_3I photodissociation. Their results indicated that the vibrational excitation is much stronger and broader in the photodissociation of CF_3I compared to CH_3I. The vibrational distribution of CF_3 in the I^* channel, which was observed to be very similar to that in the I channel, was found to peak at a rather high quantum number $n = 6$ with an average internal energy of 0.68 eV and a fwhm of ~0.87 eV. Recently, Felder[4(c)] reexamined the experiments of van Veen *et al.* at 248 nm by using a same type of method but with a higher resolution. The CF_3 vibrational

distributions of Felder in both the I^* and I channels were found to be much narrower with lower average internal energies than those of van Veen *et al.* This suggested that the results of van Veen *et al.* involved a substantial instrumental broadening. Moreover, the vibrational structure corresponding to the progression of the ν_2 mode of CF_3 (with a maximum at $n = 4$) was resolved in the I^* channel, giving the first evidence for the dominant excitation of the ν_2 vibrational mode in the CF_3I photodissociation. In the subsequent study[4(b)] at the same wavelength, Felder was able to determine the internal energy distributions of the CF_3 fragment for the I^* and I channels in correlation with the initial excitation (to either $^3Q_0$ or $^1Q_1$) by examining the translational energy dependence of the spatial anisotropy.

Theoretical works on the photodissociation of CF_3I have mostly focused on the dynamics on the $^3Q_0$ potential energy surface (PES). Different types of model $^3Q_0$ potentials were constructed with a major effort to reproduce the vibrational distribution of CF_3 in the I^* channel determined from the early experiments of van Veen *et al.*[3] van Veen *et al.*,[3] in their theoretical part of the work, performed a coupled-channel calculation assuming a collinear pseudotriatomic dissociation involving one CF_3 vibrational mode (the ν_2 umbrella vibration) and two excited states (the $^3Q_0$ and $^1Q_1$ states). The model PESs were constructed to reproduce the resolved spectra of Gedanken[23] as well as correct vibrational frequencies and dissociation limit. The calculated vibrational distribution for the I^* channel was substantially colder and much narrower than their experimental distribution, but recently found to be in fair agreement with the high resolution results of Felder.[4] For the I channel, the calculation predicted a bimodal vibrational distribution (a lower energy one from excitation to the $^1Q_1$ state and a higher energy one from the curve crossing from the $^3Q_0$ to $^1Q_1$ state), which is inconsistent with the experimentally observed[3,4] broad structureless distributions. Further theoretical works have been performed by two groups considering only the $^3Q_0$ excited state. Clary[5] used a

multidimensional $^3Q_0$ PES involving two CF_3 vibrational modes (ν_1 and ν_2), and predicted preferential excitation of the combination levels of the ν_1 and ν_2 modes. This is inconsistent with the ν_2 vibrational progression observed in the recent experiments of Felder.[4] The calculated vibrational distribution at 248 nm was found to be much narrower with a slightly lower average internal energy than the early experimental results of van Veen *et al.* Schinke and coworkers[6(a)] modified the model $^3Q_0$ potential of van Veen *et al.* by employing a distance dependent local vibration frequency and were able to obtain good agreement with the experimental results of van Veen *et al.* The calculated vibrational distribution of Schinke and coworkers, consequently, does not agree with the recent experimental results of Felder.

III. Experimental

Details of the experimental method and apparatus have been reported previously[16,18] and only a brief description will be given here. A single-stage pulsed acceleration TOF mass spectrometer fitted with an effusive sample source was used in combination with a linearly-polarized pulsed laser with a fwhm of ca. 20 ns. The TOF apparatus was equipped with a 6.0 mm diameter discrimination pinhole placed in front of the detector to reduce the detection solid angle. The laser propagation axis, the effusive sample beam, and the detection axis of the TOF apparatus (i.e., the line containing the center of the discrimination pinhole with its direction parallel to the acceleration electric field) were aligned to intersect in the center of the ionization-acceleration region of the TOF apparatus at mutually orthogonal angles. The experimental procedure used is as follows.

At time zero, a focused laser pulse photodissociates the sample molecules at one-photon level and state-selectively ionize (within the same laser pulse) the resulting iodine atom fragment via resonance-enhanced multiphoton ionization (REMPI). After a delay time τ_d (1.50 μs), the iodine ions produced are accelerated toward the detector by applying

an acceleration electric-field pulse of ca. 1010 V/cm with a fwhm of ca. 1 μs to the ionization-acceleration region of the TOF apparatus. After passing through a ca. 78 cm field-free drift region and the discrimination pinhole, the accelerated photoions are detected using a microchannel plate detector as a function of their TOF with respect to the timing of the acceleration electric-field pulse.

Experiments were performed at two wavelengths, 304.02 nm (17 μJ/pulse) and 304.67 nm (30 μJ/pulse), to photodissociate the sample molecules and also to state-selectively ionize the resulting I^* and I fragments, respectively, within the same laser pulse. TOF distributions were measured at two laser polarization angles, $\alpha = 0°$ and 90°, with respect to the detection axis. CF_3I was purchased from Aldrich and used without further purification. Neat vapor of CF_3I at room temperature and at a stagnation pressure of ~0.2 Torr was introduced through 1 mm diameter Teflon tubing and the pressure in the TOF apparatus was kept at ~1.5×10^{-6} Torr. The instrumental parameters, that are necessary to obtain the photofragment recoil velocity distribution from the measured TOF distributions, were determined by studying the photodissociation of I_2 as described previously.[16,18]

IV. Results and Analysis

A. Methods of Data Analysis

Details of the experimental principles and the data analysis methods have been described elsewhere.[16,17(b),18] In our method, the TOF of the photoion is related to the component of the photofragment recoil velocity along the detection axis due to the use of the time-delayed pulsed-acceleration. Moreover, due to the dramatic reduction of the detection solid angle by the use of the discrimination pinhole, the component of the photofragment recoil velocity observed in our method becomes very close to the photofragment recoil speed itself. This greatly enhances the velocity resolution of the

method and also facilitates the deconvolution procedure to separately obtain the angular and the recoil speed distribution from the measured TOF distributions.

The TOF distributions h^{α}(TOF) of the iodine ion measured at two laser polarization angles, $\alpha = 0°$ and 90°, with respect to the detection axis were used to determine the lab. recoil velocity distribution $f(v,\theta)$ of the iodine fragment (in the selected electronic state depending on the laser wavelength), where v is the photofragment recoil speed in the lab. frame and θ is the lab. recoil angle with respect to the electric vector of the photolysis light. In this transformation method, we used an explicit form of the instrumental detection function with well-characterized instrumental parameters (see Refs. 16, 17(b), and 18 for details). The lab. recoil velocity distribution $f(v,\theta)$ was assumed[17(b),18] to have the same form as that of the c.m. distribution[25-28] resulting from a one-photon electric dipole transition:

$$f(v,\theta) = \frac{1}{4\pi} [1 + \beta(v) P_2(\cos\theta)] g(v) \qquad (1)$$

where $P_2(\cos\theta) = (3\cos^2\theta - 1)/2$ is the second order Legendre polynomial. As given by Eq. (1), the photofragment recoil velocity distribution can be characterized by the recoil speed distribution $g(v)$ and the anisotropy parameter $\beta(v)$. Note that we express the anisotropy parameter as a function of v. This form is more general (compared to writing it as a constant parameter that is valid only for an instantaneous photodissociation process) in representing various types of photodissociation processes such as the case involving a wide range of dissociation times[17] or more than one transitions with different polarization[16] as in the present case. The value of β must lie in the range $-1 \le \beta \le 2$. The two limiting values -1 and 2 correspond to the case of prompt dissociation with the direction of the parent molecule transition dipole moment lying perpendicular and parallel to the dissociation bond axis, respectively.

For more detailed analysis, the photofragment recoil speed distributions at two recoil angles, $f(v, \theta = 0°)$ and $f(v, \theta = 90°)$, were reconstructed from $g(v)$ and $\beta(v)$ according to

Eq. (1). This is useful (1) to take into account the angular dependence of the instrumental broadening due to the thermal velocity of the parent molecule, and (2) to examine the angular dependence of the c.m. recoil velocity distribution and thus that of the c.m. translational energy release distribution. From the integrated intensities of $f(v,\theta)$, $I_{\parallel}$ and $I_{\perp}$ at $\theta = 0°$ and 90°, respectively, one can determine the average anisotropy parameter $\bar{\beta}$ according to the following equation:

$$\bar{\beta} = \frac{I_{\parallel} - I_{\perp}}{0.5\, I_{\parallel} + I_{\perp}} \tag{2}$$

The translational energy release distribution $G^{\theta}(E_t)$ at each recoil angle θ was obtained from $f(v,\theta)$ by applying the momentum conservation rule:

$$E_t = \frac{m_I(m_I + m_R)}{2m_R}\, v^2 \tag{3}$$

$$\text{and thus } G^{\theta}(E_t) = \frac{m_R}{m_I(m_I + m_R)}\, \frac{f(v,\theta)}{v} \tag{4}$$

where E_t is the sum of the translational energies of the iodine atom and the CF_3 radical, and m_I and m_R are the mass of the iodine atom and that of the CF_3 radical, respectively.

B. TOF and Recoil Velocity Distributions

Fig. 1 shows the TOF distributions of the iodine ion produced at 304.02 nm with the laser polarization angle $\alpha = 0°$ and 90° with respect to the detection axis. At this wavelength, only the excited state iodine atom I^* can be ionized via REMPI.[16] The peaks at the longer and shorter TOF correspond to the iodine ions recoiling toward (getting less acceleration) and away from (getting more acceleration) the detector, respectively. Note the strong bias in the observed ion signal at the two laser polarization angle. The ion signal is ~15 times stronger at $\alpha = 0°$ than $\alpha = 90°$. This suggests that the I^* atoms recoil predominantly along the direction of the electric vector of the laser light.

Fig. 2 gives the TOF distributions of the iodine ion measured at 304.67 nm, where the ground state iodine atom can only be ionized by REMPI.[16] Contrasting to the I^* channel, the ion signal in this channel is observed to be similar at the two laser polarization angles, indicating that the angular distribution of the I atom is nearly isotropic.

From the measured TOF distributions shown in Figs. 1 and 2, recoil velocity distributions of the I^* and I atoms in the lab. frame are determined (see Refs. 16-18 for details of the transformation method) and presented in Figs. 3 and 4, respectively. In order to show the accuracy of the transformation method used, TOF distributions are simulated using the recoil velocity distributions shown in Figs. 3 and 4, and compared with the experimental distributions in Figs. 1 and 2. As shown, the experimental TOF distributions agree well with the simulations.

As shown in Figs. 3 and 4, the recoil speed distributions $g(v)$ of the I^* and I atoms have similar shape with no significant structures. The fact that both recoil speed distributions are very sharp and have their maxima at high recoil speeds indicates that both iodine atoms are produced from repulsive potential energy surfaces which result in highly nonstatistical energy partitioning toward the translational mode. This is the typical characteristic of the electronic states of the alkyl iodide in the *A* band. The anisotropy parameters $\beta(v)$ of the I^* and I atoms are strongly contrasting in two aspects. While the value of β of the I^* atom is very close to the limiting value 2 of the parallel transition (except for the low recoil speed region where β is lower due to the instrumental broadening effect as will be discussed later), that of the I atom is close to zero. Moreover, the recoil speed dependence of β is observed to be different. The β value of the I^* atom is nearly constant except for the low recoil speed side where β decreases with v. In contrast, the I atom shows that its value of β is decreasing as v increases over the whole range of v.

The different values of the anisotropy parameter observed in the two dissociation channels can be interpreted in accord with the known nature[21] of the three possible

electronic transitions in the *A* band of the alkyl iodide, i.e., the transitions to the $^3Q_1$, $^3Q_0$, and $^1Q_1$ states. Due to the symmetry of CF_3I, each transition must be polarized either parallel ($^3Q_0$) or perpendicular ($^3Q_1$ and $^1Q_1$) to the C-I bond axis. Moreover, the time scale of the dissociation is expected to be much shorter than the rotation time of the parent molecule as observed in the photodissociation[8,9] of CH_3I (cf., this is implied by the observed sharp recoil speed distributions with high recoil speeds). Thus, each type of transition must lead to a value of the anisotropy parameter that is close to its limiting value (i.e., 2 and -1 for parallel and perpendicular transitions, respectively). Based on the observed high parallel type anisotropy and above consideration, we assign the I^* channel to the parallel $^3Q_0 \leftarrow N$ transition which correlates to I^*. The near zero value of β observed in the I channel can then be attributed to a mixed transition of the parallel $^3Q_0 \leftarrow N$ and the perpendicular $^3Q_1 \leftarrow N$ transition. The formation of the I atom from the $^3Q_0 \leftarrow N$ transition is thus attributed to the curve crossing to the $^1Q_1$ state which dissociates into I, as suggested[11-13,20] for CH_3I. Above assignments are made in accord with the MCD results[23] on CF_3I. According to the MCD results, the highest lying $^1Q_1$ state, which crosses with the $^3Q_0$ state, is expected to carry no absorption strength in the 304 nm region, and the lowest lying $^3Q_1$ state, which does not cross with the $^3Q_0$ state, has its absorption maximum around the 304 nm region. Therefore, in the 304 nm region, the I^* atom can be produced only from the $^3Q_0 \leftarrow N$ transition while the I atom can be produced from both the $^3Q_1 \leftarrow N$ and $^3Q_0 \leftarrow N$ transitions. This is different from the case at 248 nm where the perpendicular transition to the $^1Q_1$ state can contribute to the formation of I^* via curve crossing from the $^1Q_1$ to the $^3Q_0$ state as observed by Felder.[4(b)]

The recoil speed dependence of the anisotropy parameters in the I^* and I channels is related to the instrumental broadening due to the thermal velocity of the parent molecule as well as the angular dependence of the c.m. recoil velocity distributions. The dependence observed in the I^* channel is consistent with the instrumental broadening effect. As

discussed previously,[16,17(b),18] the broadening due to the parent molecule velocity is in general asymmetric and it depends on the recoil angle when the angular distribution is anisotropic. In the lab. frame, photofragments with the c.m. recoil angle deviating from the direction of the detection can be detected upon addition of the parent molecule velocity. Since the thermal velocity distribution of the parent molecule is isotropic, this gives more broadening toward the slower recoil speed. Therefore, it is expected that the more photofragments recoil away from the detection axis, the more serious is this asymmetric broadening. For anisotropic angular distributions, this must lead to more reduction of the spatial anisotropy (i.e., a decrease in the absolute value of β) in the lower recoil speed side. This is consistent with the recoil speed dependence of β observed in the I^* channel (see Fig. 3). Based on the fact that the observed value of β is constant (and very high) on the high recoil speed side, we conclude that the c.m. recoil velocity distribution of the I^* atom is independent of the recoil angle (i.e., the c.m value of β is constant). This interpretation is consistent with our assignment of the pure parallel transition for the I^* channel. Since the I^* atoms are produced from a single transition that must result in a very short dissociation time due to the repulsive nature of the excited state, the value of the anisotropy parameter in the c.m. frame would be constant and very close to the limiting value.

Different from the I^* channel, the instrumental broadening effect in the I channel is expected to be nearly independent of the recoil angle because the observed angular distribution of the I atom is nearly isotropic ($\beta \sim 0$). Therefore, the recoil speed dependence of β in this channel can be attributed to the angular dependence of the c.m. recoil velocity distribution due to the different recoil velocity distributions of the parallel and perpendicular components. Note that the value of β above the peak recoil speed is negative and that below the peak recoil speed is positive (see Fig. 4). This suggests that the I atoms produced from the perpendicular transition have higher recoil speeds than those from the parallel transition.

C. Determination of the Branching Ratio and the c.m. Translational Energy Release

As discussed in the previous section, three components contribute to the photodissociation of CF_3I in the 304 nm region. Below, we estimate the relative contributions and the c.m. translational energy release of the three components. Similar methods have been used in our previous study[16] on the photodissociation of C_2F_5I.

Fig. 5 shows recoil velocity distributions of the I^* and I atoms at two recoil angles, θ = 0° and 90°, with respect to the electric vector of the photolysis light. These distributions are reconstructed from the recoil velocity distributions shown in Figs. 3 and 4. From the integrated intensities at the two recoil angles, we obtain the average anisotropy parameter $\bar{\beta}$ to be 1.66±0.02 for I^* and -0.09±0.05 for I according to Eq. (2). As discussed in the previous section, we attribute the I^* channel to the pure parallel transition ($^3Q_0 \leftarrow N$) in accord with the MCD results.[23] Thus, the reduced value of $\bar{\beta}$ in this channel (compared to the limiting value 2) is attributed to the vibrational and rotational motions of the parent molecule during the dissociation process and the instrumental broadening due to the parent molecule velocity. Relative contributions of the parallel and the perpendicular transition to the I channel ($X_{||}$ and $X_{\perp}$, respectively) can be estimated from the following relation:[16]

$$\bar{\beta} = X_{||}\,\beta_{||} + X_{\perp}\,\beta_{\perp} \qquad (5)$$

where $\beta_{||}$ and $\beta_{\perp}$ are the anisotropy parameters for the parallel and perpendicular transitions, respectively. In order to take into account the reduction of the anisotropy parameter due to the parent molecule motions and the instrumental broadening, we use the value of $\bar{\beta}$ observed in the I^* channel as a reference value. Thus, taking $\beta_{||}$ = 1.66 and $\beta_{\perp}$ = -0.83, we obtain $X_{||}$ = 0.30 and $X_{\perp}$ = 0.70. Therefore, the contribution of the $^3Q_1 \leftarrow N$ transition is found to be dominant over that of the $^3Q_0 \leftarrow N$ transition in the formation of I.

Fig. 6 gives the translational energy release distributions $G^{\theta}(E_t)$ of the I^* and I channels at two recoil angles. Representative values of these distributions are summarized

in Table 1. In the I^* channel, the translational energy release distribution at $\theta = 90°$ has a smaller value of the average translational energy release $\langle E_t \rangle_\theta$ with a larger width than that at $\theta = 0°$. This angular dependence can be attributed to the instrumental broadening effect due to the parent molecule velocity as discussed in the previous section. For this channel, we take the value of $\langle E_t \rangle_\theta$ at $\theta = 0°$ as an average c.m. translational energy release and the width at the same recoil angle as an upper limit of the c.m. distribution. As indicated by the observed high parallel type anisotropy, the I^* atoms recoil predominantly along the detection axis at $\theta = 0°$ and thus the instrumental broadening is expected[29] to be nearly symmetric at this recoil angle.

The average c.m. translational energy release of the parallel and the perpendicular components in the I channel ($\langle E_t \rangle_{||}$ and $\langle E_t \rangle_\perp$, respectively) can be estimated[16] as follows. In this channel, the angular distribution of the photofragment is given by:

$$I(\theta) = \frac{1}{4\pi}[1 + \bar{\beta} P_2(\cos\theta)]$$
$$= \frac{X_{||}}{4\pi}[1 + \beta_{||} P_2(\cos\theta)] + \frac{X_\perp}{4\pi}[1 + \beta_\perp P_2(\cos\theta)] \qquad (6)$$

According to this equation, both the parallel and the perpendicular component contribute to the observed signal at each recoil angle. Thus, we write the following equations to take into account the relative contributions of the two components to the observed values of $\langle E_t \rangle_\theta$:

$$\langle E_t \rangle_{\theta=0°} = 35.8 \text{ kcal/mol} = 0.98 \langle E_t \rangle_{||} + 0.02 (\langle E_t \rangle_\perp - \Delta) \qquad (7)$$

$$\langle E_t \rangle_{\theta=90°} = 36.8 \text{ kcal/mol} = 0.31 (\langle E_t \rangle_{||} - \Delta) + 0.69 \langle E_t \rangle_\perp \qquad (8)$$

The first and second terms on the right sides of these two equations correspond to the contributions of the parallel and perpendicular components, respectively. A parameter Δ takes into account the instrumental broadening effect in the following manner. For the parallel component, the average translational energy release is assumed to be the same as the c.m. value at $\theta = 0°$, but it will be smaller by Δ at $\theta = 90°$ due to the instrumental

asymmetric broadening. For the perpendicular component, an opposite is true, i.e., the value at $\theta = 0°$ will be smaller than the c.m. value by a similar amount. Using the value of Δ measured for the I^* channel (1.3 kcal/mol), we find that $\langle E_t \rangle_{||}$ = 35.8 kcal/mol and $\langle E_t \rangle_{\perp}$ = 36.9 kcal/mol.

D. Energy Partitioning and the Dissociation Energy

Internal excitation energy of the CF_3 radical (E_{int}) can be determined from the c.m. translational energy release (E_t) by using the following energy conservation relations:

$$E_{avl} = h\nu - D_o^o + E_{int}^p = E_t + E_{int} \text{ for the I channel} \quad (9)$$

$$E_{avl}^* = E_{avl} - E_{so} = E_t^* + E_{int}^* \text{ for the } I^* \text{ channel} \quad (10)$$

where $h\nu$ is the photon energy, D_o^o is the dissociation energy of the ground state CF_3I into the ground state CF_3 radical and the I atom at 0 K, E_{int}^p is the internal energy of the parent molecule, and E_{so} is the spin-orbit excitation energy of the iodine atom (21.7 kcal/mol). To use these relations, one must know the values of D_o^o and E_{int}^p. We use the known values[30] of the vibrational frequencies and the rotational constants of CF_3I to calculate the average internal energy of the parent molecule $\langle E_{int}^p \rangle$ at room temperature. Using a Boltzmann distribution of population as usual,[20] we obtain the value of $\langle E_{int}^p \rangle$ to be 2.1 kcal/mol, of which 0.9 kcal/mol is due to rotation and 1.2 kcal/mol is due to vibration. Up to date, two different values of D_o^o have been reported. van Veen *et al.*[3] reported a value of 53.0 kcal/mol from the TOF photofragment translational spectroscopy study of CF_3I at 248 nm. Recently, Felder[4(a)] reexamined the experiment of van Veen *et al.* using the same technique but with a better resolution, and obtained a higher value of D_o^o (55.2 kcal/mol). As suggested by Felder, it is likely that the value of van Veen *et al.* is erratic due to the large instrumental broadening involved in their experiment. However, the value of D_o^o reported by Felder seems to disagree with our results. Using his value of D_o^o, we

obtain the available energy for the I* channel (E_{avl}*) to be 19.2 kcal/mol. This is lower than the average c.m. translational energy released measured for this channel ($\langle E_t^* \rangle$ = 19.9 kcal/mol), inconsistent with the energy conservation. One could blame that the discrepancy is rather small if all the available energy has been released in translation. However, since only a part of the initial internal energy of the parent molecule will be released in translation, the discrepancy seems to be rather large (say on the order of ~2 kcal/mol). Therefore, we estimate an upper limit of D_o^o using the measured value of $\langle E_t^* \rangle$ as given below.

We expect that the initial internal energy of the parent molecule ($\langle E_{int}^p \rangle$) and the excess energy provided by the photon energy ($h\nu - D_o^o - E_{so}$) will contribute to the translational energy release in different manners. Thus we write an equation: $\langle E_t^* \rangle = E_t^{thermal} + X\,(h\nu - D_o^o - E_{so})$, where $E_t^{thermal}$ is the contribution from the thermal internal energy of the parent molecule and X is an unknown parameter ($0 \le X \le 1$). The value of $E_t^{thermal}$ can be estimated as follows. Since two out of three rotational degrees of freedom correspond to the orbital angular motion of the collision complex, we estimate the contribution of the parent molecule rotational motion to $E_t^{thermal}$ to be about 0.6 kcal/mol (2/3 x 0.9 kcal/mol). We expect that only a fraction of the vibrational energy of the parent molecule, that is initially deposited in the C-I dissociation coordinate, will be released in translation. Considering the total number of the vibrational modes (9) compared to that actively related to the dissociation coordinate (3), about 30% of the initial vibrational energy (0.3 x 1.2 kcal/mol = ~0.4 kcal/mol) would appear in translation. Thus, the value of $E_t^{thermal}$ is estimated to be about 1.0 kcal/mol with an uncertainty of a few tenth of kcal/mol. Using this value of $E_t^{thermal}$ and taking $X = 1$, we obtain an upper limit of D_o^o to be 53.4 kcal/mol.

Although the value of D_o^o estimated above is only an upper limit, this value seems to be very close to the real value. Our value is about 2 kcal/mol smaller than the value of Felder[4(a)] and slightly larger than the value of van Veen *et al.*[3] As discussed by Felder, his value of D_o^o is an upper limit. Since the experiment of van Veen *et al.* was found (by Felder) to involve a significant instrumental broadening, their value of D_o^o is likely a lower limit. Our value of D_o^o must then be very close to the real one (say with an error of less than 1 kcal/mol). This conclusion is also supported by the fact that our value of D_o^o agrees well with that (53.3±1.8 kcal/mol) calculated from the tabulated thermodynamic data.[30] Therefore, we use the value of 53.4 kcal/mol for D_o^o to calculate the internal excitation of the CF_3 radical. Table 2 gives a summary of the energy partitioning obtained with this value of D_o^o.

V. Discussion

Two key aspects this work addresses are (1) the effect of photon energy and (2) that of the curve crossing, in the photodissociation dynamics of CF_3I in the *A* band. We will compare the results of this work in the 304 nm region with the recent results of Felder[4(b)] at 248 nm to examine the theoretical predictions from model calculations.[3,5,6] It must be noted that for the purpose of the present study the internal energy of CF_3 must be measured in correlation with the initial electronic excitation as well as the final state of the iodine fragment as was done in the two experiments. Since all the experimental values for the internal energy of the CF_3 fragment are determined from the measured translational energies, the values at 248 nm to be used in the remaining part of this section are those recalculated using our value of D_o^o (53.4 kcal/mol).

Before we consider the internal excitation of CF_3, it is worthwhile to compare the electronic transitions and the curve crossing processes involved in the photodissociation at the two wavelengths. As observed by Felder[4] (and also by van Veen *et al.*[3] and Person *et*

al.[24]), two excited states, the $^3Q_0$ (~88%) and $^1Q_1$ (~12%) states, contribute to the absorption at 248 nm and a nonadiabatic curve crossing takes place between the two excited states. As a result, both the I* and I channels at 248 nm consist of two components due to the excitation to the $^3Q_0$ and $^1Q_1$ states. At ~304 nm as described early, the absorption is to the $^3Q_0$ and $^3Q_1$ states and the curve crossing takes place from the $^3Q_0$ to the $^1Q_1$ state. Thus, the I* channel has one component due to the excitation to the $^3Q_0$ state while the I channel consists of two components due to the excitation to the $^3Q_1$ state and the curve crossing from the $^3Q_0$ to $^1Q_1$ state (see Table 2). Therefore, there are two common dissociation processes at the two wavelengths, i.e., the dissociation into $CF_3 + I^*(^2P_{1/2})$ due to the excitation to the $^3Q_0$ state and the dissociation into $CF_3 + I(^2P_{3/2})$ due to the curve crossing from the initial $^3Q_0$ state to the $^1Q_1$ state. We will thus consider the vibrational excitation for these two dissociation processes in terms of the photon energy dependence and the effect of the curve crossing.

We first discuss the photon energy dependence of the vibrational excitation on the $^3Q_0$ PES which dissociates into $CF_3 + I^*$. A key aspect to be tested is the strong photon energy dependence of the vibrational excitation of CF_3 predicted from theoretical calculations. As shown in Fig. 7, the theoretical values of the average vibrational energy of CF_3 reported by van Veen *et al.* and Clary[5] are considerably high at high photon energies and decrease rather steeply as the photon energy decreases, finally reaching zero near a photon energy of ~34000 cm^{-1} (~300 nm). Schinke and coworkers[6(a)] also predicted a similar dependence with a steeper slope. As compared in Fig. 7, the experimental results indeed show such a strong photon energy dependence. The experimental value[4(b)] at 248 nm is very high lying in between the two theoretical values, and it is very close to zero at ~304 nm. In fact, our result at ~304 nm is in perfect agreement with both calculations since the observed average internal energy is almost entirely due to the initial thermal energy of the parent molecule as discussed early. From

the slope of the photon energy dependence, it can be seen that the dependence predicted by van Veen *et al.*[3] is in slightly better agreement with the experimental results. This suggests that the sole consideration of the ν_2 mode, as assumed in the model calculation of van Veen *et al.*, could be sufficient to describe the dynamics of the vibrational excitation on the $^3Q_0$ PES. This conclusion is also supported by the progression of the ν_2 mode observed at 248 nm by Felder.[4] The slightly stronger photon energy dependence predicted by Clary[5] is probably due to the predicted extensive excitation of the combination bands of the ν_1 and ν_2 modes, as opposed to the Felder's experimental observation.

Given the agreement described above, it is important to discuss the origin of the strong photon energy dependence of the vibrational excitation on the $^3Q_0$ PES of CF_3I. As discussed by van Veen *et al.*,[3] the vibrational excitation is determined by *structural change upon photoexcitation* and *final state interaction* (i.e., translational-vibrational energy transfer) *during the dissociation*. According to the model calculation of van Veen *et al.*,[3] parts of the $^3Q_0$ PES excited at high and low photon energies, as determined by Frank-Condon overlap, are only slightly different in terms of the ν_2 vibration coordinate, i.e., the initially prepared C-F_3 distance (within the assumption of "collinear triatomic dissociation") is similar to the equilibrium distance of the final CF_3 fragment at the low photon energy, and it is only slightly longer at the high photon energy. In the absence of final state interaction, this would result in a weak photon energy dependence of the vibrational excitation. However, as discussed by van Veen *et al.*,[3] the presence of a strong final state interaction amplifies the difference in the vibrational excitation at the high and low photon energies, resulting in a strong photon energy dependence. Recently, Schinke and coworkers[6] examined the effects of these two factors separately by comparing dynamics of the vibrational excitation in different model $^3Q_0$ potentials for CF_3I, and reached a similar conclusion. In the view of the results of Schinke and coworkers, one could determine the strength of the translational-vibrational coupling (i.e., the final state interaction) from the

measured photon energy dependence. This must be very important to construct a realistic PES.

We now discuss the vibrational excitation in the $^3Q_0$ component of the $CF_3 + I$ channel which results from the curve crossing. This dissociation process involves two excited state PESs. While the early dissociation takes place on the initially prepared $^3Q_0$ PES, the later dissociation occurs on the $^1Q_1$ PES due to the curve crossing. Since the dynamics on the $^3Q_0$ PES is well understood as discussed above, it is possible to get some insight on the effect of the curve crossing. In Fig. 7, the average internal energies measured for this dissociation process are compared with those for the dissociation along the $^3Q_0$ potential. As shown, both processes lead to similar strong photon energy dependence in terms of their slopes. However, the average internal energies at both photon energies are considerably higher when the curve crossing takes place. A possible explanation for this observation is as follows. The fact that both dissociation processes give similar slopes of photon energy dependence suggests that the observed strong dependence is predominantly due to the dynamics on the $^3Q_0$ potential. The extra internal excitation observed in the dissociation involving the curve crossing must then be attributed to the dynamics of the curve crossing as well as the dynamics on the $^1Q_1$ potential.

The experimental results described above are inconsistent with the theoretical results of van Veen *et al.*,[3] which predicted that the curve crossing has little effect in the vibrational excitation. From the model potentials of van Veen *et al.*, it appeared that the curve crossing occurred at a larger C-I distance where the equilibrium geometries of the two potentials were similar, thus resulting in no significant change in the vibrational excitation. A most likely candidate for the discrepancy between the experiment and the theory is the multidimensional nature of the curve crossing process as opposed to the one-dimensional (involving only the a_1-symmetry ν_2 vibration) model calculation of van Veen *et al.*[3] As suggested by several studies,[2,12,24,32,33] an *e*-symmetry vibration must be

involved to induce the curve crossing (via vibronic coupling) due to the different symmetry of the two excited electronic states involved, i.e., $^3Q_0$ of A_1 and $^1Q_1$ of E. It is therefore possible that the curve crossing process itself involves excitation of *e*-symmetry vibrations, resulting in more vibrational excitation as observed in the present study. The fact that the observed increase in the average internal energy of CF_3 due to the curve crossing (~1500 and ~2000 cm^{-1} at 248 and 304 nm, respectively) is higher than the two *e*-symmetry vibrational frequencies of CF_3 (1251 and 512 cm^{-1} for the asymmetric C-F stretching and bending vibrations, respectively)[5] suggests that further vibrational excitation might occur due to the dynamics on the $^1Q_1$ potential after the curve crossing. In addition, it is interesting to point out that the increase of the internal excitation due to the curve crossing is observed to be more (by ~500 cm^{-1}) at the lower photon energy. This suggests that upon and/or after the curve crossing the dissociation with a higher energy leads to less internal excitation, in contradiction to a simple expectation. This seems to indicate a subtle aspect of the curve crossing and the subsequent dynamics on the $^1Q_1$ potential. Presumably, the curve crossing takes place in different regions of the PESs depending on the initial excitation, thus resulting in different dynamics.

In conclusion, we have shown that details of the photodissociation dynamics can be elucidated by examining photon energy dependence of internal excitation of a fragment in correlation with the initial excitation and the final state of another fragment. The present results and further similar experiments at other wavelengths seem to be very important in constructing more realistic PESs for the photodissociation of CF_3I in the *A* band. As suggested by this work and also by the recent works[4] of Felder, the photodissociation along the $^3Q_0$ potential can be described sufficiently well by considering only the ν_2 umbrella vibration. However, in order to describe the dynamics of the curve crossing and its effect in the internal excitation of CF_3, it seems necessary to construct multidimensional

PES's with more vibrational modes as suggested by the present work and the recent elegant works[2,24] of Butler and coworkers.

Acknowledgement. We thank the Office of Naval Research for support of this work.

References

(1) Guo, H.; Schatz, G. C. *J. Chem. Phys.* **1990**, *93*, 393 and references therein.

(2) Lao, K. Q.; Person, M. D.; Xayariboun, P.; Butler, L. J. *J. Chem. Phys.* **1990**, *92*, 823 and references therein.

(3) van Veen, G. N. A.; Baller, T.; de Vries, A. E.; Shapiro, M. *Chem. Phys.* **1985**, *93*, 277.

(4) (a) Felder, P. *Chem. Phys.* **1990**, *143*, 141. (b) *Ibid.* (in press).

(5) Clary, D. C. *J. Chem. Phys.* **1986**, *84*, 4288.

(6) (a) Hennig, S.; Engel, V.; Schinke, R. *J. Chem. Phys.* **1986**, *84*, 5444. (b) Untch, A.; Hennig, S.; Schinke, R. *Chem. Phys.* **1988**, *126*, 181.

(7) Hermann, H. W.; Leone, S. R. *J. Chem. Phys.* **1982**, *76*, 4766.

(8) Dzvonik, M.; Yang, S.; Bersohn, R. *J. Chem. Phys.* **1974**, *61*, 4408.

(9) Knee, J. L.; Khundkar, L. R.; Zewail, A. H. *J. Chem. Phys.* **1985**, *83*, 1996.

(10) (a) Shapiro, M.; Bersohn, R. *J. Chem. Phys.* **1980**, *73*, 3810. (b) Sharpiro, M. *J. Phys. Chem.* **1986**, *90*, 3644.

(11) Sparks, R. K.; Shobatake, K.; Carlson, L. R.; Lee, Y. T. *J. Chem. Phys.* **1981**, *75*, 3838.

(12) Barry, M. D.; Gorry, P. A. *Mol. Phys.* **1984**, *52*, 461.

(13) van Veen, G. N. A.; Baller, T.; de Vries, A. E.; van Veen, N. J. A. *Chem. Phys.* **1984**, *87*, 405.

(14) (a) Ogorzalek Loo, R.; Hall, G. E.; Haerri H.-P.; Houston, P. L. *J. Phys. Chem.* **1988**, *92*, 5. (b) Ogorzalek Loo, R.; Haerri, H.-P.; Hall, G. E.; Houston, P. L. *J. Chem. Phys.* **1989**, *90*, 4222.

(15) Black, J. F.; Powis, I. *Chem. Phys.* **1988**, *125*, 375.

(16) Hwang, H. J.; El-Sayed, M. A. *J. Chem. Phys.* **1991**, *94*, 4877.

(17) (a) Hwang, H. J.; El-Sayed, M. A. *J. Chem. Phys.* **1992**, *96*, 856. (b) *ibid.* (submitted).

(18) Hwang, H. J. *Ph. D. thesis*, 1992, University of California, Los Angeles.

(19) Kasper, J. V. V.; Pimental, G. C. *Appl. Phys. Lett.* **1964**, *5*, 231.

(20) Riley, S. J.; Wilson, K. R. *Faraday Discuss. Chem. Soc.* **1972**, *53*, 132.

(21) Mulliken, R. S. *J. Chem. Phys.* **1935**, 3, 513. *Ibid* **1940**, *8*, 382.

(22) Gedanken, A.; Rowe, M. D. *Chem. Phys. Lett.* **1975**, *34*, 39.

(23) Gedanken, A. *Chem. Phys. Lett.* **1987**, *137*, 462.

(24) Person, M. D.; Kash, P. W.; Butler, L. J. *J. Chem. Phys.* **1991**, *94*, 2557.

(25) Jonah, C. *J. Chem. Phys.* **1971**, *55*, 1915.

(26) Zare, R. N. *Mol. Photochem.* **1972**, *4*, 1.

(27) Busch, G. E.; Wilson, K. R. *J. Chem. Phys.* **1972**, *56*, 3638.

(28) Yang, S.; Bersohn, R. *J. Chem. Phys.* **1974**, *61*, 4400.

(29) This is supported by the fact that values of the average or the most probable translational energy of the iodine fragment determined by our method agree well with known literature values. For example the velocity peak positions of the iodine atoms produced in the photodissociation of I_2 in the 304 nm region (see Hwang, H. J.; El-Sayed, M. A. *J. Phys. Chem.* **1991**, 95, 8044) agree exactly with those calculated from the product states and the known dissociation energy. Moreover, the average translational energy release measured for the photodissociation reaction of CF_2IC... to $CF_2ICF + I^*$ at 304.02 nm (14.5±0.2 kcal/..., from our results to be published) agrees well with th

value measured at 308 nm (14 kcal/mol) reported by Nathanson, G. M.; Minton, T. K.; Shane, S. F.; Lee, Y. T. *J. Chem. Phys.* **1989**, *90*, 6157.

(30) Herzberg, G. *Molecular Spectra and Molecular Structure. Vol. 3. Electronic Spectra and Electronic Structure of Polyatomic Molecules*; Van Nostrand: Princeton, 1966.

(31) *JANAF Thermochemical Tables, J. Phys. Chem. Ref. Data* **1985**, *14*, Suppl. 1.

(32) Tadjeddine, M.; Flament, J. P.; Teichteil, C. *Chem. Phys.* **1987**, *118*, 45.

(33) Yabushita, S.; Morokuma, K. *Chem. Phys. Lett.* **1988**, *153*, 517.

Table 1. Angular dependence of the translational energy release distributions in the I^* and I channels from the photodissociation of CF_3I.[a]

Iodine state	Wavelength (nm)	Average anisotropy, $\bar{\beta}$	θ	$\langle E_t \rangle_\theta$	fwhm of $G^\theta(E_t)$
I^*	304.02	1.66±0.02	0°	19.9±0.2	6.1±0.2
			90°	18.6±0.2	8.3±0.2
I	304.67	-0.09±0.05	0°	35.8±0.3	10.6±0.2
			90°	36.8±0.3	9.5±0.2

[a] Energies are in kcal/mol. Uncertainties shown are ± one standard deviations of 4 to 8 measurements. Angular dependence of the translational energy release distribution observed in the I^* channel is due to angular dependence of the instrumental broadening typical for a parallel ($^3Q_0 \leftarrow N$) transition, which results from the thermal velocity of the parent molecule. The fact that the observed angular distribution of the I channel is nearly isotropic (i.e., $\beta \sim 0$) suggests that the instrumental broadening in this channel must be independent of the recoil angle θ. Therefore, the angular dependence of the translational energy release distribution observed in the I channel can be attributed to angular dependence of the c.m. translational energy release distribution resulting from a mixed transition of a parallel ($^3Q_0 \leftarrow N$) and a perpendicular ($^3Q_1 \leftarrow N$) transition. See text for more details.

Table 2. Summary on the photodissociation dynamics and the electronic transitions of CF_3I in the 304 nm region.[a]

Iodine state	Wavelength (nm)	E_{avl}	Transition type	Relative contribution	$\langle E_t \rangle$	$\langle E_{int} \rangle$	$\langle E_{int} \rangle / E_{avl}$
I*	304.02	21.0	$\parallel ({}^3Q_0 \leftarrow N)$	1.0	19.9	1.1	0.05
I	304.67	42.5	$\parallel ({}^3Q_0 \leftarrow N)$	0.30	35.8	6.7	0.16
			$\perp ({}^3Q_1 \leftarrow N)$	0.70	36.9	5.6	0.13

a Energies are in kcal/mol. $\parallel$ and $\perp$ denote the parallel and perpendicular transitions, respectively. Relative contributions shown are for each iodine state.

Figure Captions

Figure 1. TOF distributions of resonantly-ionized $I^*(^2P_{1/2})$ atoms produced from photodissociation of CF_3I at 304.02 nm for two laser polarization angles α with respect to the detection axis. The dots are experimental results and the solid curves are simulated distributions using the recoil velocity distribution in Fig. 3. The peaks in the short and longer TOF correspond to I^* atoms recoiling away from and toward the detector, respectively. Note that the *y* axis of the bottom panel is expanded 15 times. The small peaks observed at TOF = ~21.3 and ~26.4 μs in the bottom panel are due to the photodissociation of residual I_2 used for the calibration experiment.

Figure 2. The same as Fig. 1 but for $I(^2P_{3/2})$ atoms at 304.67 nm. The solid curves are calculated using the recoil velocity distribution shown in Fig. 4.

Figure 3. Lab. recoil velocity distribution of $I^*(^2P_{1/2})$ obtained from the TOF distributions in Fig. 1. The distribution is represented by the recoil speed distribution $g(v)$ and the recoil speed dependence of the anisotropy parameter $\beta(v)$ according to Eq. (1). The small peak in $g(v)$ and the large drop in $\beta(v)$ observed at v = ~1110 m/s are due to the photodissociation of I_2.

Figure 4. Lab. recoil velocity distribution of $I(^2P_{3/2})$ obtained from the TOF distributions shown in Fig. 2.

Figure 5. Lab. recoil velocity distributions of $I^*(^2P_{1/2})$ and $I(^2P_{3/2})$ at two lab. recoil angles (θ) with respect to the electric vector of the photolysis light. The dots and the solid curves correspond to $\theta = 0°$ and 90°, respectively. These are reconstructed from the recoil

velocity distributions shown in Figs. 3 and 4. The small peak at v = ~1110 m/s observed in the I^* channel is due to the photodissociation of I_2.

Figure 6. Angular dependence of the translational energy release distributions $G^{\theta}(E_t)$ of $I^*(^2P_{1/2})$ and $I(^2P_{3/2})$ as obtained from $f(v,\theta)$ in Fig. 5. To illustrate the difference between the distributions at two recoil angles, the distributions are normalized to have the unit peak height. The dots and the solid curves correspond to θ = 0° and 90°, respectively. The small peak at E_t = ~53 kcal/mol observed in the I^* channel is the photodissociation signal of I_2.

Figure 7 . Comparison of the theoretical and experimental photon energy dependence of the average internal energy of CF_3. The theoretical results of van Veen *et al.* (——, Ref. 3) and Clary (- - -, Ref. 5) are for the dissociation into $CF_3 + I^*$ due to absorption to the $^3Q_0$ state. The open and filled circles are the experimental results for the dissociation into $CF_3 + I^*$ (no curve crossing) and $CF_3 + I$ (curve crossing to the $^1Q_1$ state), respectively, resulting from absorption to the $^3Q_0$ state. The experimental results at 248 nm are those recalculated from the values of the average translational energy release reported in Ref. 4(b) using a dissociation energy D_o^o = 53.4 kcal/mol.

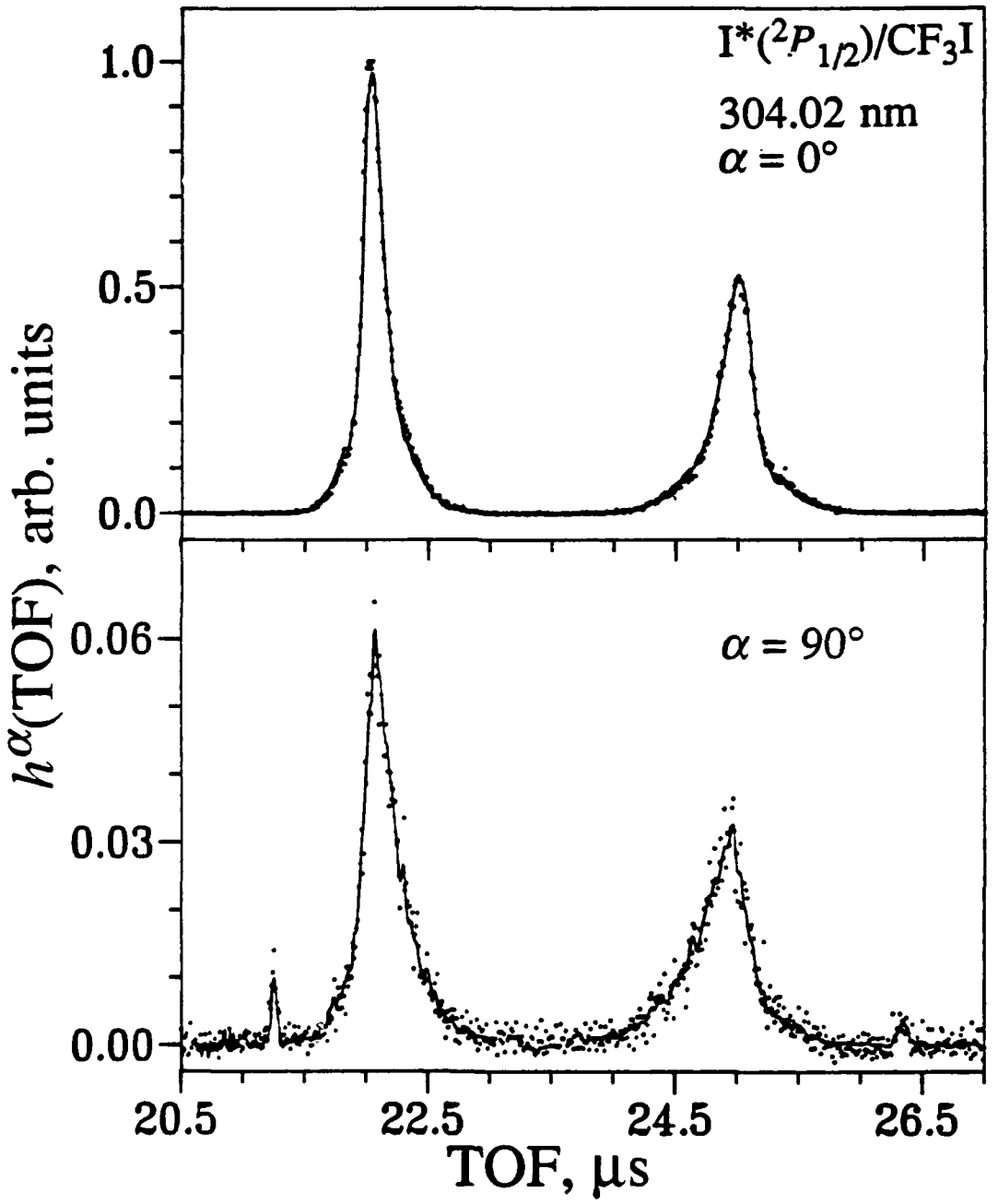

Fig. 1 H. J. Hwang and M. A. El-Sayed

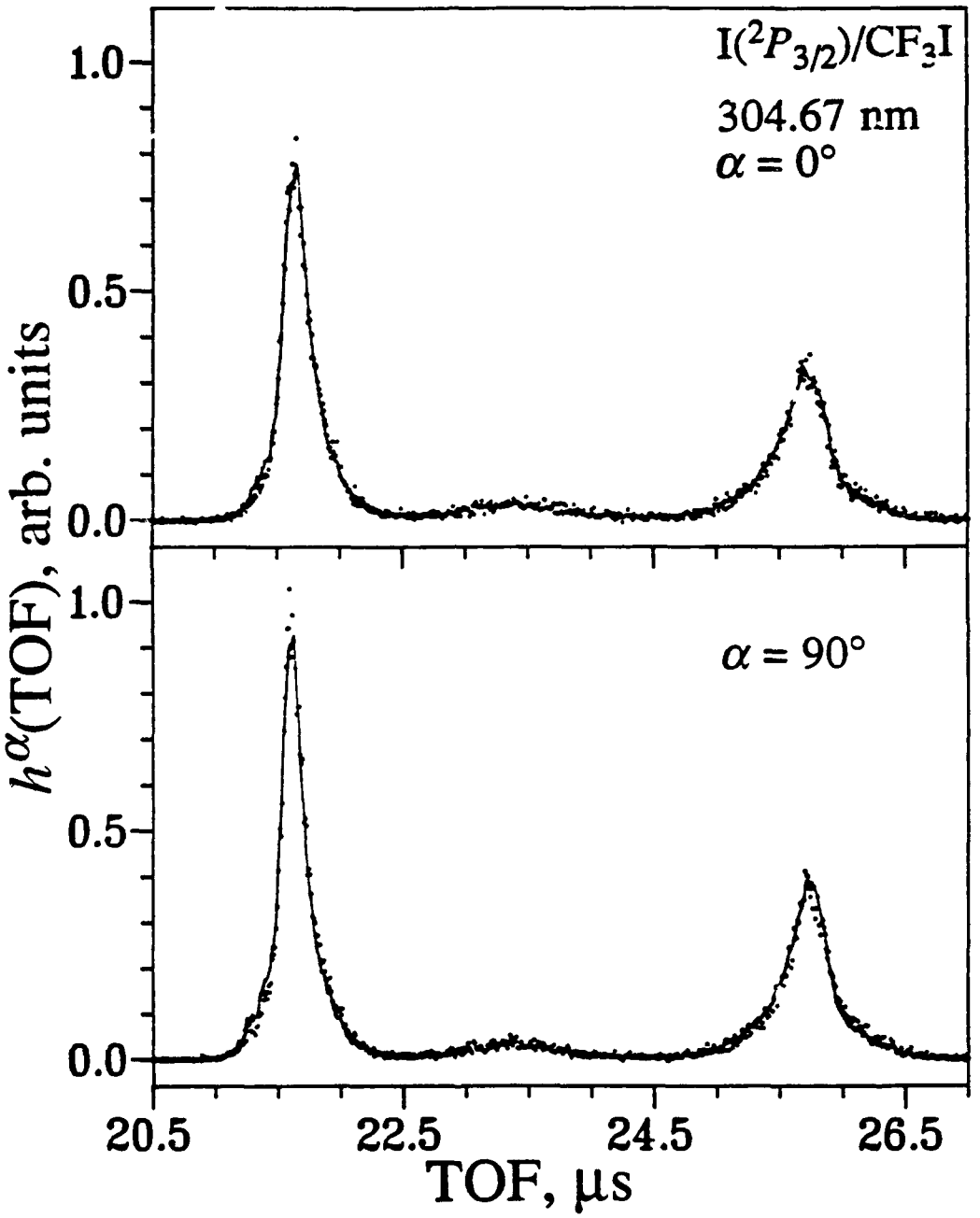

Fig. 2 H. J. Hwang and M. A. El-Sayed

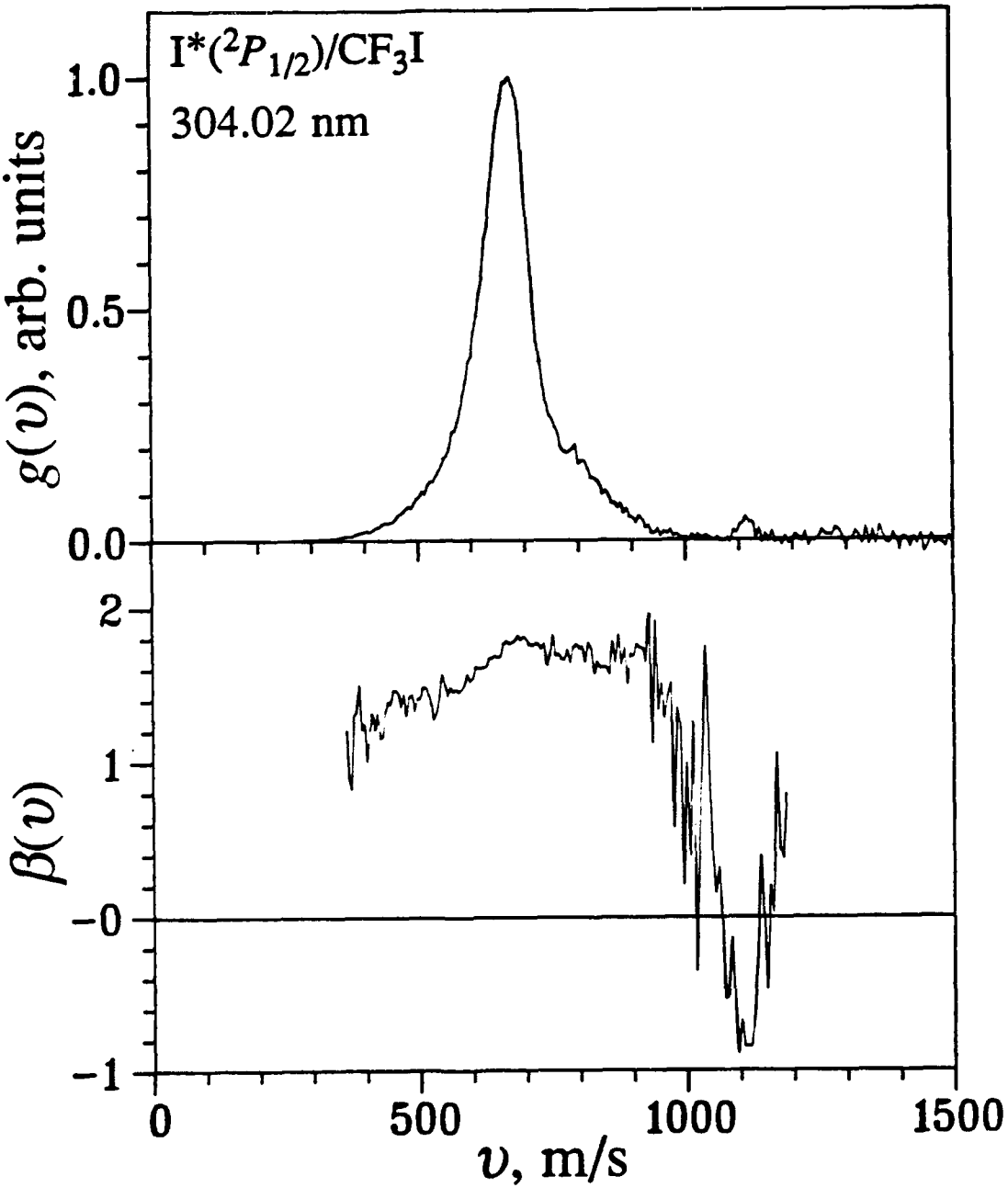

Fig. 3 H. J. Hwang and M. A. El-Sayed

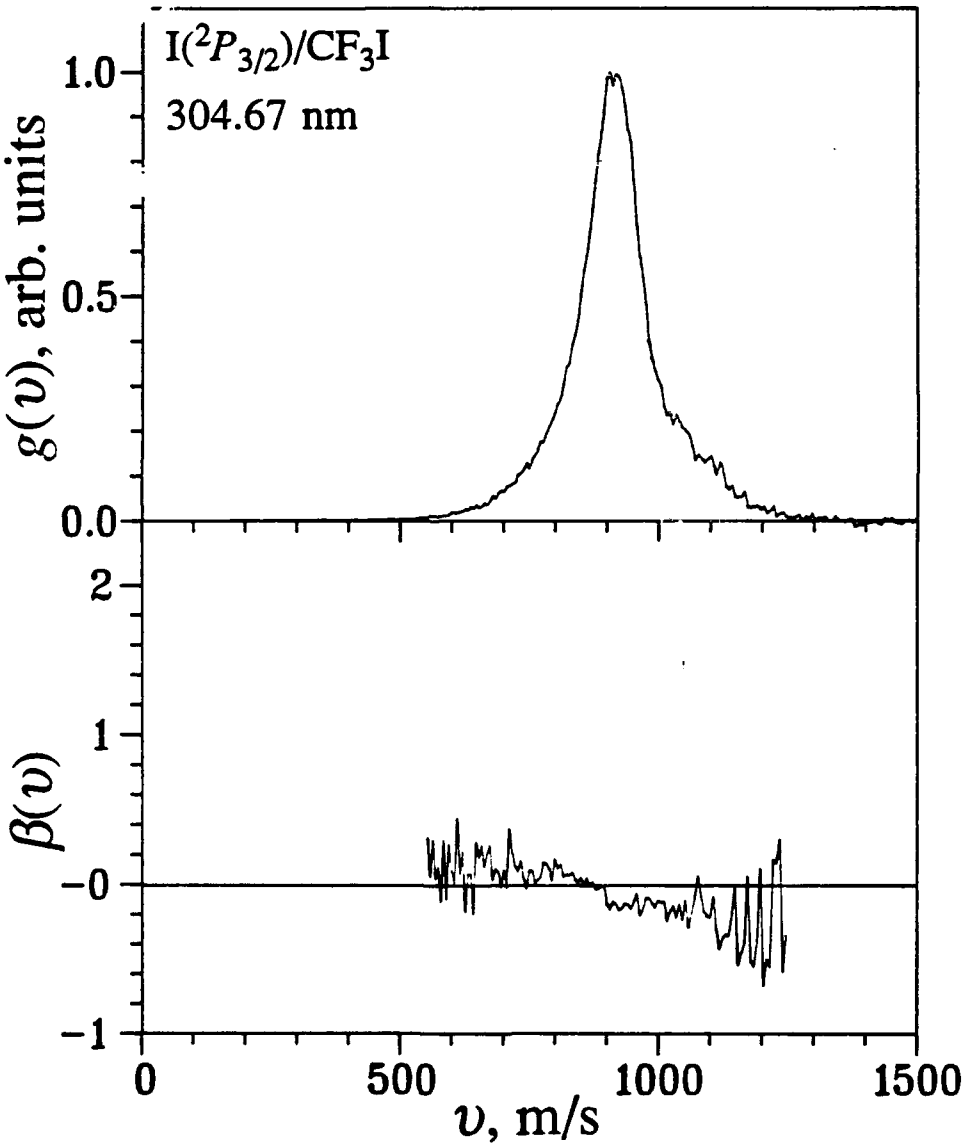

Fig. 4. H. L. Kwang and M. A. El-Sayed

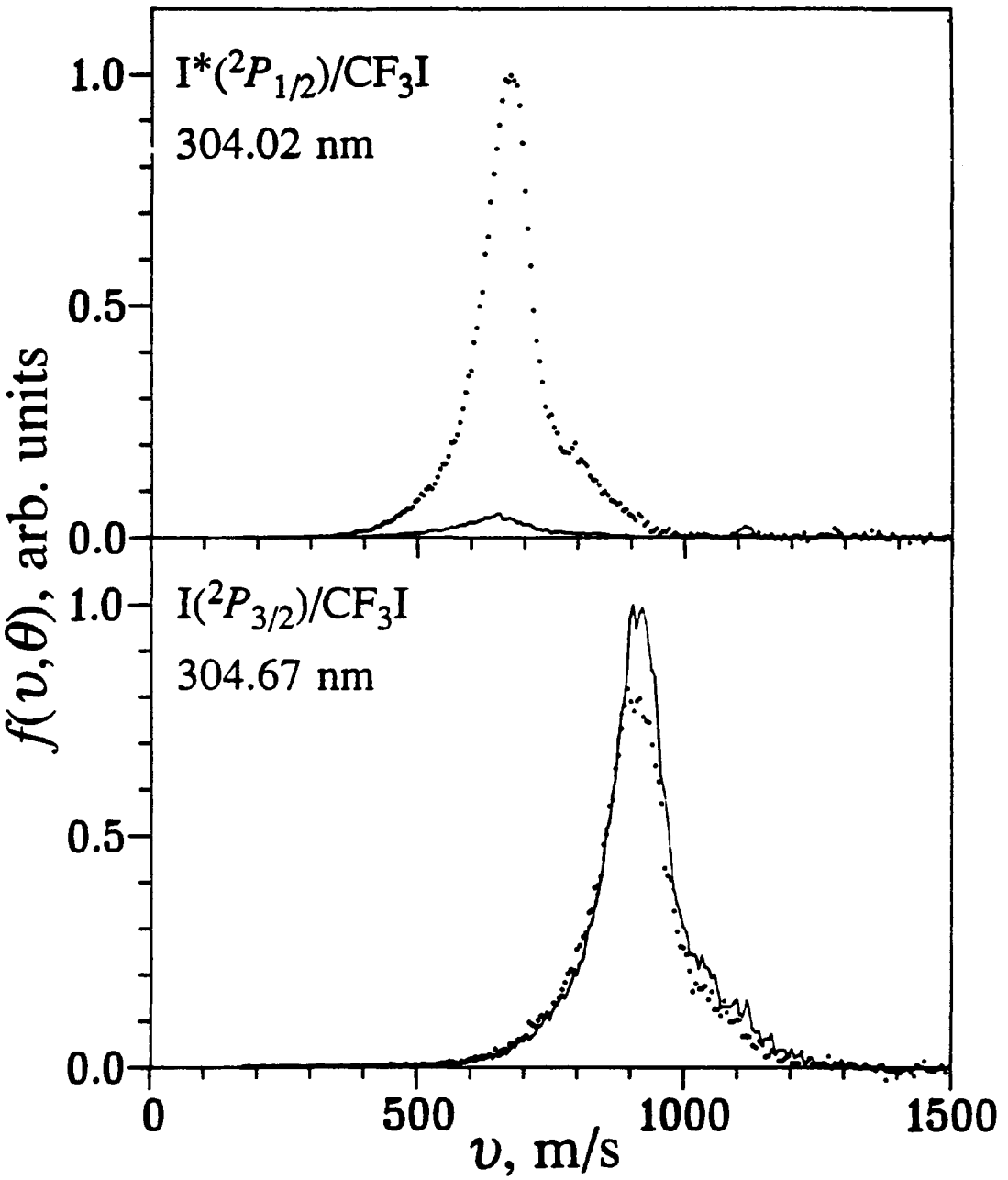

Fig. 5. H. J. Hwang and M. A. El-Sa

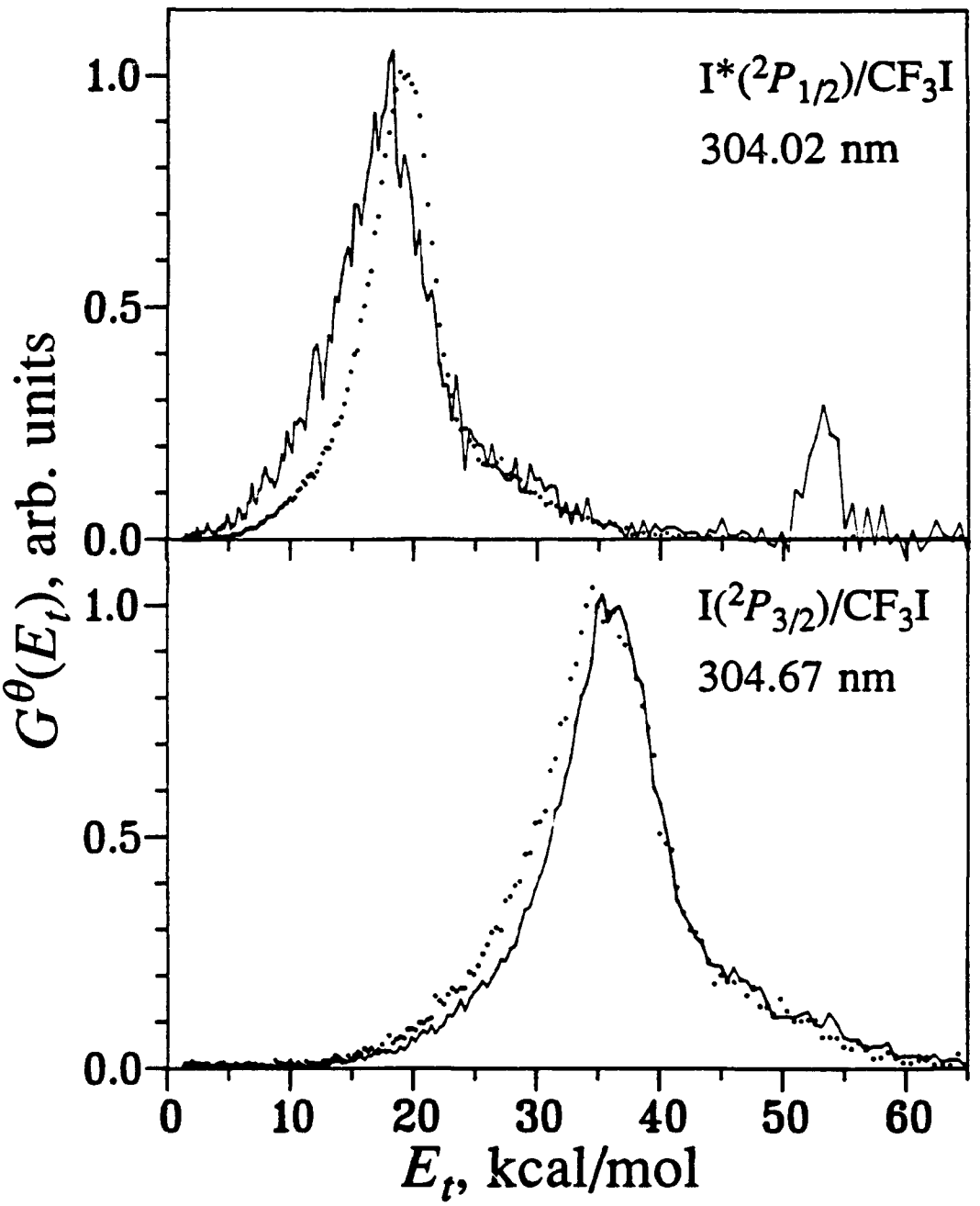

Fig. 6. H. J. Hwang and M. A. El-Sayed

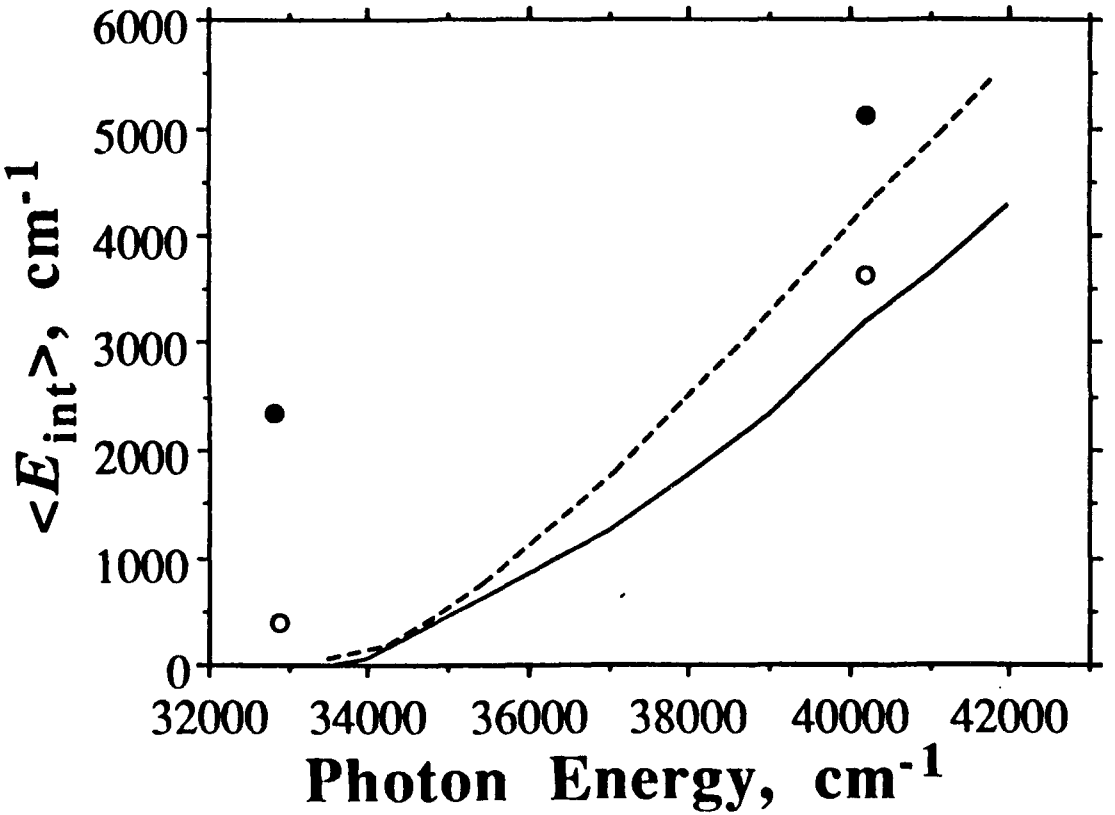

Fig. 7 H. J. Huang and M. A. El-Sayed

TECHNICAL REPORT DISTRIBUTION LIST - GENERAL

Office of Naval Research (2)*
Chemistry Division, Code 1113
800 North Quincy Street
Arlington, Virginia 22217-5000

Dr. James S. Murday (1)
Chemistry Division, Code 6100
Naval Research Laboratory
Washington, D.C. 20375-5000

Dr. Robert Green, Director (1)
Chemistry Division, Code 385
Naval Weapons Center
China Lake, CA 93555-6001

Dr. Eugene C. Fischer (1)
Code 2840
David Taylor Research Center
Annapolis, MD 21402-5067

Dr. Elek Lindner (1)
Naval Ocean Systems Center
Code 52
San Diego, CA 92152-5000

Commanding Officer (1)
Naval Weapons Support Center
Dr. Bernard E. Douda
Crane, Indiana 47522-5050

Dr. Richard W. Drisko (1)
Naval Civil Engineering
Laboratory
Code L52
Port Hueneme, CA 93043

Dr. Harold H. Singerman (1)
David Taylor Research Center
Code 283
Annapolis, MD 21402-5067

Chief of Naval Research (1)
Special Assistant for Marine
Corps Matters
Code 00MC
800 North Quincy Street
Arlington, VA 22217-5000

Defense Technical Information
Center (2)
Building 5, Cameron Station
Alexandria, VA 22314